

# Bioorthogonal, fluorogenic targeting of voltage-sensitive fluorophores for visualizing membrane potential dynamics in cellular organelles

Pavel E. Z. Klier,<sup>‡</sup> Anneliese M. M. Gest,<sup>‡</sup> Julia G. Martin,<sup>‡</sup> Ryan Roo,<sup>‡</sup> Marisol X. Navarro,<sup>‡</sup> Lauren Lesiak,<sup>‡</sup> Parker E. Deal,<sup>‡</sup> Neville Dadina,<sup>‡</sup> Jonathan Tyson,<sup>‡</sup> Alanna Schepartz,<sup>‡§</sup> and Evan W. Miller<sup>‡§†\*</sup>

Departments of <sup>‡</sup>Chemistry and <sup>§</sup>Molecular & Cell Biology and <sup>†</sup>Helen Wills Neuroscience Institute. University of California, Berkeley, California 94720, United States.

**ABSTRACT:** Electrical potential differences across lipid bilayers play foundational roles in cellular physiology. Plasma membrane voltage is the most widely studied; however, the bilayers of organelles like mitochondria, lysosomes, nuclei, and endoplasmic reticulum (ER) also provide opportunities for ionic compartmentalization and the generation of transmembrane potentials. Unlike plasma membranes, organellar bilayers, cloistered within the cell, remain recalcitrant to traditional approaches like patch-clamp electrophysiology. To address the challenge of monitoring changes in organelle membrane potential, we describe the design, synthesis, and application of LUnAR RhoVR (Ligation Unquenched for Activation and Redistribution Rhodamine based Voltage Reporter) for optically monitoring membrane potential changes in the endoplasmic reticulum (ER) of living cells. We pair a tetrazine-quenched RhoVR for voltage sensing with a transcyclooctene (TCO)-conjugated ceramide (Cer-TCO) for targeting to the ER. Bright fluorescence is observed only at the coincidence of LUnAR RhoVR and TCO in the ER, minimizing non-specific, off-target fluorescence. We show that the product of LUnAR RhoVR and Cer-TCO is voltage sensitive and that LUnAR RhoVR can be targeted to intact ER in living cells. Using LUnAR RhoVR, we use two-color, ER-localized, fast voltage imaging coupled with cytosolic Ca<sup>2+</sup> imaging to validate the electroneutrality of Ca<sup>2+</sup> release from internal stores. Finally, we use LUnAR RhoVR to directly visualize functional coupling between plasma-ER membrane in patch clamped cell lines, providing the first direct evidence of the sign of the ER potential response to plasma membrane potential changes. We envision that LUnAR RhoVR, along with other existing organelle-targeting TCO probes, could be applied widely for exploring organelle physiology.

Electrical potentials across biological membranes, including those that form membrane-bound organelles, regulate and initiate a host of physiological processes.<sup>1</sup> Although electrical potentials across external plasma membranes have been extensively studied, organelle membrane potentials remain relatively under-explored, by comparison. The membranes of organelles, ensconced within the confines of the cellular membrane, are difficult to access with electrodes, making determination of organelle membrane potential difficult.<sup>2-4</sup> While optical methods for monitoring changes in or measuring values of *plasma* membrane potentials are a powerful complement to electrode-based methods, delivering and targeting voltage-sensitive dyes to specific, internal organelle membranes for visualizing organelle membrane potential is an outstanding challenge.

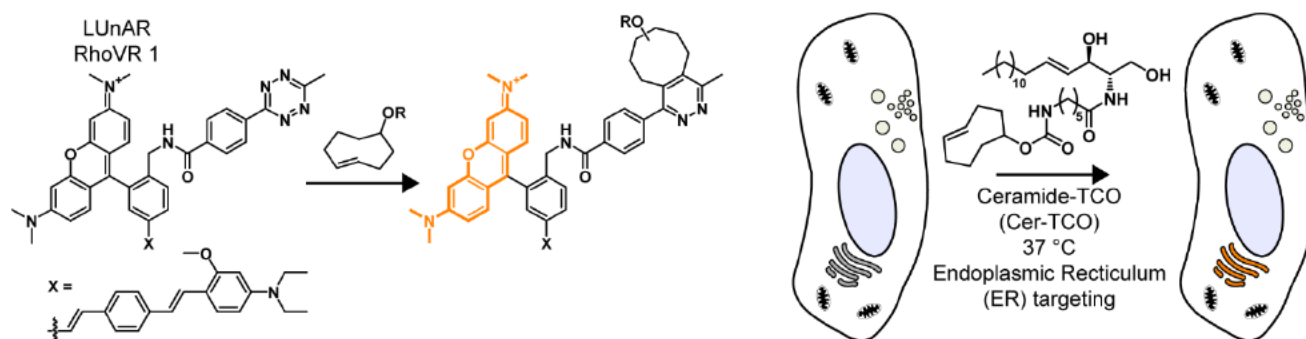
Many strategies exist to target voltage sensitive fluorophores to mitochondria: most rely on lipophilic, cationic groups which accumulate in the mitochondrial matrix in a potential-dependent fashion. Approaches to other organelles are limited. Recent efforts to optically measure membrane potential of internal organelles have used DNA nanodevices<sup>5</sup> or genetic targeting with small molecule

quenchers to target lysosomal membranes.<sup>6</sup> Other approaches use completely genetically encoded voltage-sensitive fluorescent proteins which express in both external and internal membranes to track membrane potential, but labeling can be ambiguous because of variable expression levels.<sup>7</sup> A need exists for robust approaches to monitoring membrane potentials of cellular organelles.

We wondered whether we might adapt VoltageFluor dyes for delivery to organelle membranes and take advantage of the photoinduced electron transfer (PeT) voltage-sensing mechanism to monitor membrane potential in organelles. Most existing VoltageFluors are designed to be cell impermeant for measuring cellular membrane potential and thus do not effectively stain organelle membranes.<sup>8</sup> However, we recently found that modifications to a rhodamine-based voltage reporter (RhoVR) enabled passage through cell membranes and localization to mitochondria.<sup>9</sup>

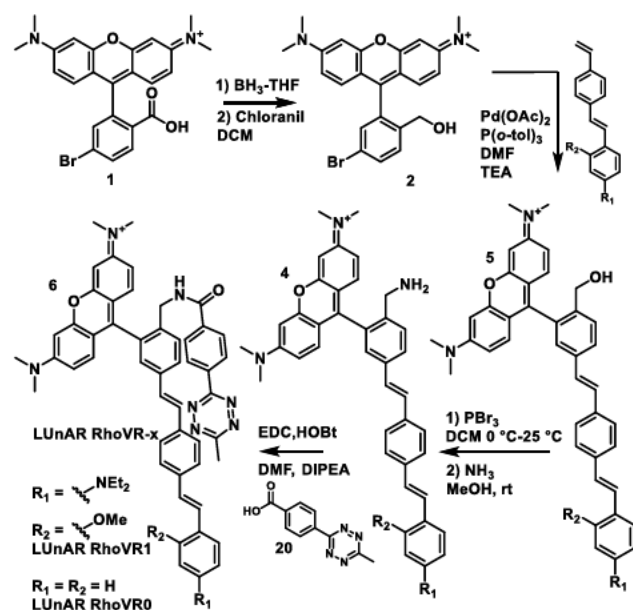
Fluorescent dyes can be targeted to subcellular locations either through charge,<sup>10-12</sup> covalently attached groups specific to a subcellular location,<sup>13</sup> genetic targeting of protein constructs,<sup>14-18</sup> or bioorthogonal chemistry in which one reaction partner is attached to a targeting group and another

## Scheme 1. Structures of LUnAR RhoVR and Cer-TCO for targeted delivery of RhoVRs to organelles



A small molecule rhodamine voltage sensor functionalized with a tetrazine quencher (LUnAR RhoVR 1) reacts with a targeted transcyclooctene (TCO) to form a covalent adduct with unquenched fluorescence. When this reaction is performed in live cells with a targeted transcyclooctene, for example ceramide-TCO, the small molecule voltage sensor is targeted to the membrane of interest with quenched fluorescence from any off-target localization.

## Scheme 2. Synthesis of LUnAR RhoVRs



is attached to the fluorescent probe to allow targeting in living cells.<sup>29</sup> A VoltageFluor targeted using bioorthogonal chemistry would be targetable to multiple subcellular locations using different targeted reaction partners. We selected a transcyclooctene (TCO)/tetrazine click reaction to use for subcellular targeting of VoltageFluors due to its rapid reaction kinetics<sup>20-22</sup> and the ability of tetrazines to quench the fluorescence of xanthene dyes.<sup>23-25</sup> Fluorescence becomes unquenched after the tetrazine group reacts with a strained alkene to form a covalent adduct, tethering unquenched dye to the subcellular location targeted by the alkene.

To realize this strategy, we made a Ligation Unquenched for Activation and Redistribution Rhodamine Voltage Reporter (LUnAR RhoVR). In this approach, a TCO is targeted to the membrane of interest using either a chemical targeting group or genetically targeted protein, after which the voltage reporter reacts with the targeted TCO to covalently bind it to the membrane of interest. Off-target background fluorescence is minimized because of quenching by

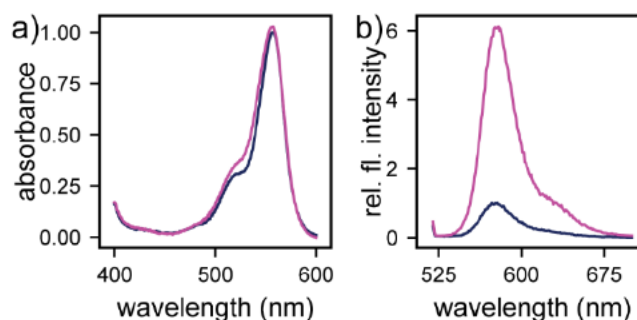


**Figure 1.** Optical properties of LUnAR RhoVR before and after reaction with transcycloocteneol (TCO-ol). a) Plot of absorbance vs wavelength for LUnAR RhoVR1 before (dark blue) and after (magenta) reaction with transcycloocteneol. b) Plot of fluorescence emission vs. wavelength for LUnAR RhoVR 1 before (dark blue) and after (magenta) reaction with transcycloocteneol from the samples shown in a. Spectra were acquired in ethanol with 0.01% HCl. LUnAR RhoVR 1 (200  $\mu$ M) was reacted with transcyclooctenol (10 mM) in 5:1 water:dioxane and then diluted to 500 nM for spectral measurements.

the unreacted tetrazine group, (Scheme 1). After synthesizing and screening four different rhodamine-tetrazine linker chemistries for fluorescence turn-on (Figure S1), we settled on an amide linkage between the RhoVR and the tetrazine due to its superior turn-on and synthetic compatibility with published VoltageFluor syntheses (Scheme 1).

The synthesis of tetrazine-containing LUnAR RhoVR proceeds from a reduction of a brominated carboxytetramethyl rhodamine (1)<sup>8</sup> to the corresponding alcohol (2) followed by a Heck reaction with a molecular wire. The alcohol is then converted to a primary amine and coupled using carbodiimide chemistry to 3-methyl-6-carboxyphenyl tetrazine(24)<sup>26</sup> to give LUnAR RhoVR 1 (Scheme 2). A similar synthesis with a molecular wire lacking aniline and methoxy groups gives LUnAR RhoVR 0, a voltage insensitive compound which serves as a useful control for cellular studies.<sup>27-29</sup>

LUnAR RhoVR 1 and 0 possess absorbance and emission spectra characteristic of tetramethyl rhodamine, with absorbance centered at 557 nm and an emission maximum of

**Table 1. Reactions of LUnAR with Transcyclooctenes**

| RhoVR <sup>a</sup> | TCO                         | $\Phi_f^b$   |
|--------------------|-----------------------------|--------------|
| LUnAR 1            | ---                         | 0.042        |
| LUnAR 1            | TCO-ol                      | 0.26 (6.2×)  |
| LUnAR 1            | TCO-PEG <sub>25</sub> -Halo | 0.28 (6.7×)  |
| LUnAR 1            | Cer-TCO                     | 0.20 (4.8×)  |
| LUnAR o            | ---                         | 0.032        |
| LUnAR o            | TCO-ol                      | 0.32 (10.0×) |
| LUnAR o            | Cer-TCO                     | 0.17 (5.3×)  |

**a** The indicated LUnAR RhoVR (200  $\mu$ M) was reacted with the indicated transcyclooctene (10 mM) in 5:1 water:dioxane and then diluted to 500 nM in ethanol with 0.01% HCl for spectral measurements. **b** Quantum yield of fluorescence. Values in parenthesis indicate fold increase over unreacted RhoVR.

578 nm (**Figure 1, Figure S2**). The fluorescence of LUnAR RhoVR 1 increases 7-fold upon reaction with TCO-ol (25); LUnAR RhoVR o increases 10-fold (**Figure 1, Table 1**). Although the fluorescence increases, the absorbance shows very little change before and after reaction with TCO, indicating that the increase in brightness results primarily from a change in the quantum yield of fluorescence. Similar turn-on ratios are achieved with TCO compounds bearing HaloTag ligands and ceramide (**Table 1**).

We first tested a HaloTag targeting system for targeting LUnAR RhoVRs to both the exterior and interior leaflets of the plasma membrane. TCO tethered to a HaloTag chloroalkane ligand via a flexible polyethyleneglycol (PEG) linker would first be localized to HaloTag. Then, treatment with LUnAR RhoVR would result in labeling of HaloTag proteins (**Scheme 1**). LUnAR RhoVR<sub>1</sub> labels the plasma membrane when HaloTag is localized to the outer leaflet of the plasma membrane (**Figure S3a-c**); however, when HaloTag is localized to the endomembrane via prenylation<sup>30</sup> (**Figure S4**), we observe very low levels of cellular fluorescence, likely because the long PEG linkers used to ensure voltage sensitivity of RhoVRs in HaloTag targeted systems<sup>29</sup> prevent substantial internalization of RhoVR (**Figure S3d-f**). Labeling of cells expressing the same endomembrane HaloTag show robust fluorescence when labeled with the cell-permeable JF646-HaloTag ligand, supporting this hypothesis (**Figure S3f-h**).

We verified the voltage-sensitivity of the product of LUnAR RhoVR 1 and TCO by reacting TCO-PEG<sub>25</sub>-Halo (25) with LUnAR RhoVR 1 *in vitro* and applying this to cells expressing outer leaflet HaloTag (**Figure S5**).<sup>29</sup> Patch clamp electrophysiology on these cells reveal that LUnAR RhoVR 1 / TCO conjugates respond to membrane potential change, with a sensitivity of approximately 21% ( $\pm$  0.72%, S.E.M. for n = 3 cells, **Figure S5**).

After establishing the voltage sensitivity of LUnAR RhoVR<sub>1</sub>-TCO conjugates at the outer leaflet of the plasma membrane, we turned to the organelle specific lipid-TCO developed by the Schepartz lab for their High Density

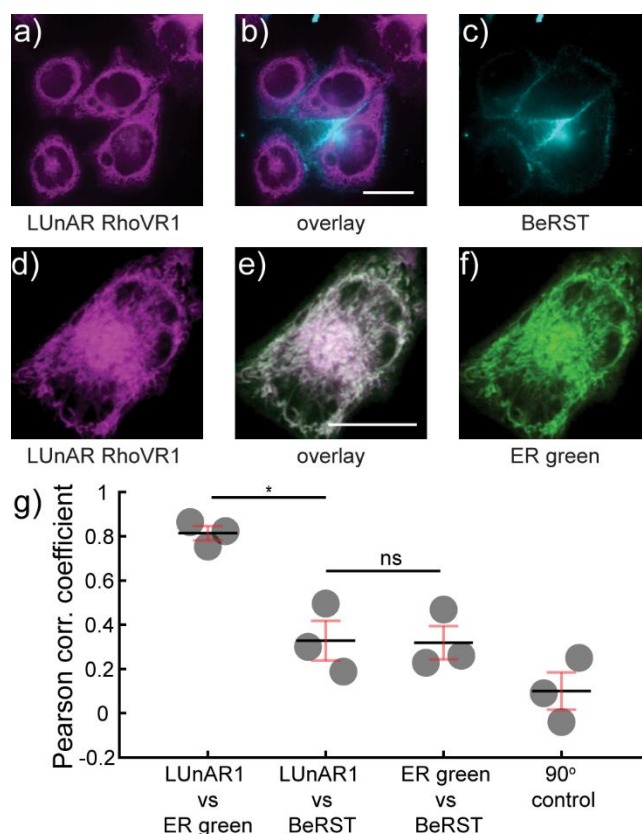


**Figure 2.** LUnAR RhoVR 1 + Cer-TCO localize to the endoplasmic reticulum of HeLa cells. Confocal slices of HeLa cells pre-incubated with Cer-TCO followed by labeling with **a**) LUnAR RhoVR 1 (magenta) and **c**) the plasma membrane marker BeRST (cyan). **b**) An overlay of the two signals shows no significant overlap. Scale bar is 20  $\mu$ m. Confocal slices of HeLa cells pre-incubated with Cer-TCO followed by labeling with **d**) LUnAR RhoVR 1 (magenta) and **f**) ER Tracker Green (green). **e**) An overlay of the two signals shows overlap in white. Scale bar is 20  $\mu$ m. **d**) Plot of Pearson's coefficients for colocalization analysis of LUnAR RhoVR 1 and ER green or BeRST. 90° control indicates analysis in which one of the images has been rotated 90° during the colocalization analysis. \* indicates p < 0.05; "ns" indicates p > 0.05 (student's t-test, two tailed unequal variance).

Environmentally-sensitive probes (HIDE probes)<sup>31</sup> to target LUnAR RhoVRs to organelles. We loaded HeLa cells with a ceramide-TCO that targets the endoplasmic reticulum (ER), followed by loading with LUnAR RhoVR 1 or LUnAR RhoVR o. Cell treated with Cer-TCO followed by LUnAR RhoVR 1 show strong fluorescence associated with internal structures (**Figure 2a, Figure S6, S7**). LUnAR signal colocalizes with the ER (Pearson's coefficient of 0.8 with ER Tracker Green, **Figure 2d**) and shows negligible plasma membrane staining (Pearson's coefficient of 0.35 with membrane-associated BeRST,<sup>32</sup> **Figure 2d, Figure S6**). Similar colocalization analysis reveals minimal colocalization with mitochondria (when using mitotracker deep red as a marker for mitochondria<sup>10, 33</sup>) or Golgi (using GalNAc - BFP as Golgi marker).<sup>34</sup> The voltage insensitive control compound, LUnAR RhoVR o, shows similar cellular localization (**Figure S6, S8**).

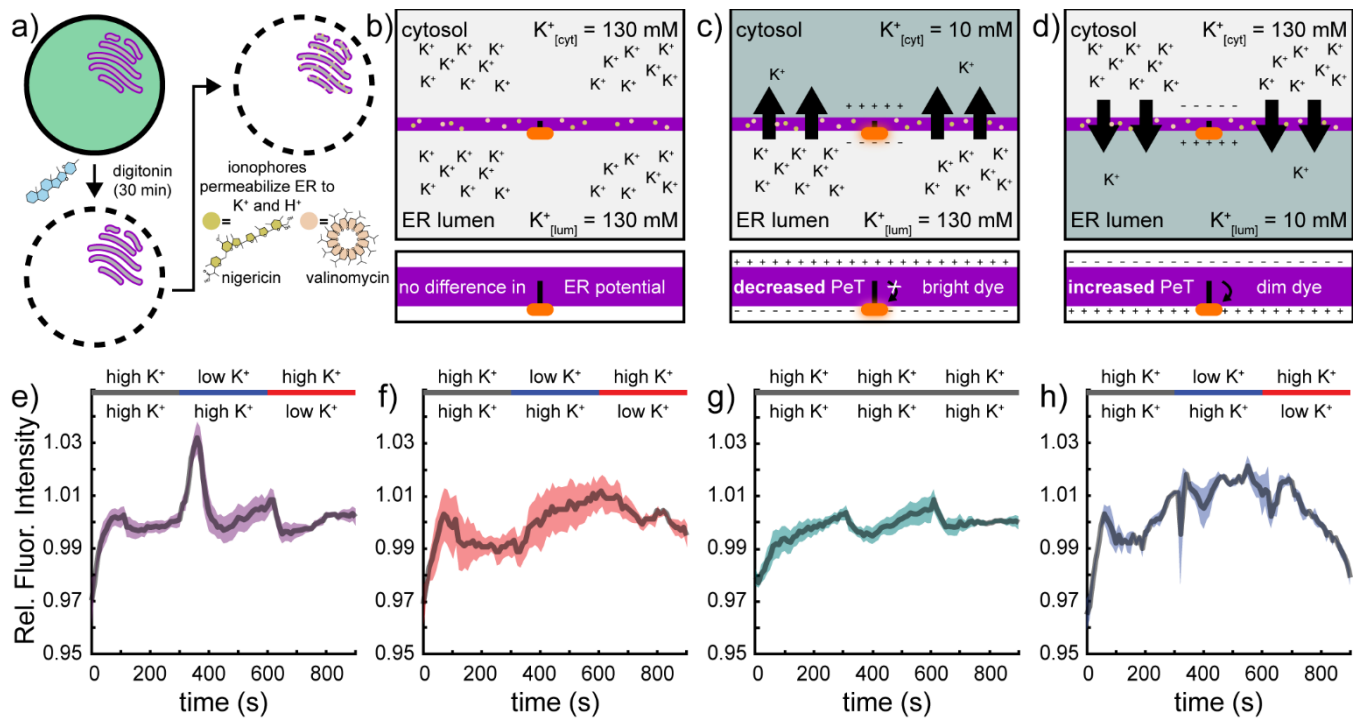


**Figure 3.** LUnAR RhoVR1 senses voltage changes across the ER membrane. **a)** Schematic representation of permeabilization of plasma membranes with digitonin, resulting in loss of calcein fluorescence (green) but retention of LUnAR RhoVR1 staining in ER, treatment with ionophores valinomycin (beige) and nigericin (yellow), and modulation of  $[K^+]$  to change ER membrane potential. **b)** When cytosolic and luminal  $[K^+]$  is equal, there is no difference in membrane potential. **c)** When the cytosolic  $[K^+]$  is switched to 10 mM, valinomycin facilitates the diffusion of  $K^+$  ions out of the ER lumen, resulting in a net negative luminal potential, decreased PeT, and increased RhoVR fluorescence. **d)** When cytosolic  $[K^+]$  is returned to 130 mM,  $K^+$  again diffuses down its concentration gradient, resulting in a net positive luminal potential, increased PeT, and decreased RhoVR fluorescence. **e-h)** Plots of relative RhoVR fluorescence intensity vs. time for Cer-TCO loaded, LUnAR RhoVR1 stained HeLa cells with **e)** digitonin-permeabilized plasma membranes or **f)** intact plasma membranes. Grey bars indicate high  $[K^+]$  (130 mM) in both cytosolic/external and luminal spaces, blue bars indicate low cytosolic/extracellular  $[K^+]$  (10 mM) with high luminal  $[K^+]$ , and red bars indicate high cytosolic/extracellular  $[K^+]$  with low luminal  $[K^+]$ . **g)** Plot of relative RhoVR fluorescence intensity for cells as in (e), but with a constant high  $[K^+]$  (130 mM) perfusion. **h)** Plot of relative RhoVR fluorescence intensity for cells as in (e), but with voltage-insensitive LUnAR RhoVR o in place of LUnAR RhoVR1. Data represent mean values (solid lines)  $\pm$  error (S.E.M.) for  $n = 9, 5, 4$ , or 3 for conditions e, f, g, and h, respectively.

Having established that LUnAR RhoVR1 can label to ER via reacting with pre-localized Cer-TCO (Figure 2) and that the reaction product of LUnAR RhoVR1 + TCO is voltage sensitive (Figure S5), we next sought to determine whether LUnAR RhoVR1 is voltage sensitive in the ER membrane. Because of the difficulty associated with patch clamp electrophysiological calibration of ER membrane potential in living cells, we modified a previously reported literature method for inducing voltage changes in intracellular membranes.<sup>6</sup> In our method (Figure 3a, Figure S9), cells loaded with LUnAR RhoVR1 targeted to the ER via Cer-TCO are first treated briefly with digitonin to selectively permeabilize the cell membrane, but not organelle membranes. Digitonin permeabilizes cholesterol-rich membranes.<sup>35</sup> The plasma membrane contains up to 50% cholesterol content;<sup>36-37</sup> while ER membranes contain only about 5% cholesterol content.<sup>38-39</sup> Thus, the digitonin treatment selectively permeabilizes the plasma membrane while leaving the ER membrane intact.

We established plasma permeability by co-incubation with calcein-AM: cells with intact cell membranes retained

calcein-AM fluorescence, while cells with permeabilized membranes showed little to no calcein fluorescence (Figure 3a).<sup>40</sup> After treatment with digitonin, cells are incubated in a buffer mimicking the intracellular environment (high  $[K^+]$  of 130 mM) and containing the potassium ionophores valinomycin and nigericin which allows  $K^+$  ions to equilibrate along their electrochemical gradient (Figure 3b).

Subsequently, a solution of low  $[K^+]$  (10 mM) is perfused onto the cells (Figure 3c) while fluorescence images are taken over time (Figure 3e-h, S10). A short voltage transient is induced due to the different  $K^+$  concentrations on either side of the ER membrane and high  $K^+$  permeability induced by valinomycin and nigericin, resulting in a net negative potential on the luminal side of the ER (Figure 3c). Accompanying this hyperpolarization is a transient increase in LUnAR RhoVR1 fluorescence of approximately 5% (Figure 3e). When a high  $[K^+]$  solution is perfused back on the cells, the potential across the ER membrane is positive on the luminal side (Figure 3d), and a small decrease in fluorescence occurs (Figure 3e). This response is likely



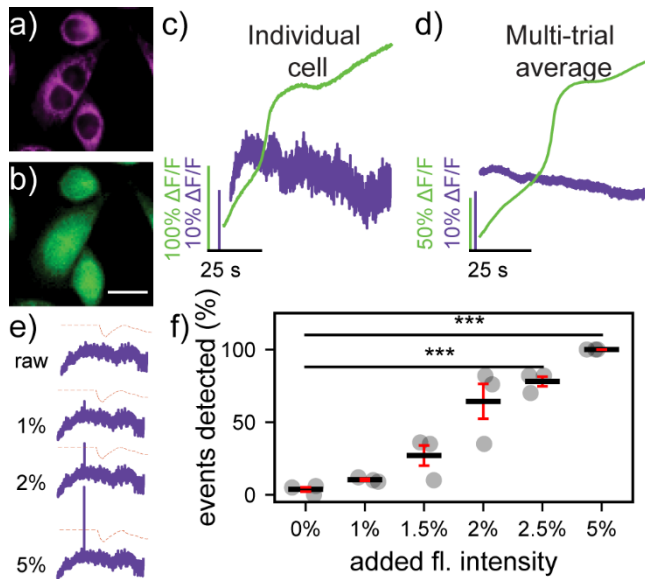


**Figure 4.** ER membrane potential does not change during  $\text{Ca}^{2+}$  release in HeLa cells. **a)** Fluorescence image of HeLa cells treated with Cer-TCO and **a)** LUnAR RhoVR1 to stain the ER and **b)** OGB-AM to visualize  $\text{Ca}^{2+}$  transients. Scale bar is 20  $\mu\text{m}$ . Plots of LUnAR RhoVR1 fluorescence (purple) and OGB fluorescence (green) vs time after histamine (100  $\mu\text{M}$ ) stimulation from a single HeLa cell 100  $\mu\text{M}$  histamine stimulation (100  $\mu\text{M}$ ). Data are for either **c)** a single cell or **d)** the average across 3 different coverslips. **e)** Adding a fluorescence change of 0%, 1%, 2%, and 5% into the raw trace of a single cell (purple trace) and the threshold for 10 standard deviations above the local average fluorescence (dashed orange trace) used for detection. **f)** Plot of the fraction of individual cells in a single coverslip that have an event detected above the threshold shown in **c)** on the raw fluorescence data from histamine trials as well as raw data where a single frame has an added fluorescence change of the amount indicated on the x-axis. \*\*\* indicates  $p < 0.001$  (student's t-test, 2-tailed, unequal variance)

smaller than the response to the initial hyperpolarization due to incomplete equilibration of the ER lumen with the low  $[\text{K}^+]$  solution and thus a smaller magnitude of the reverse voltage transient.

The increase in fluorescence associated with ER lumen hyperpolarization is only observed in cells with permeabilized plasma membranes; non-permeabilized cells in the same dish, identified by their high intracellular calcein fluorescence, do not respond to differing  $[\text{K}^+]$  perfusion (**Figure 3f**, **Figure S11**). In separate control experiments, perfusion with identical high  $[\text{K}^+]$  solutions results in no fluorescence change (**Figure 3g**). Finally, if the high/low  $[\text{K}^+]$  perfusion is repeated with voltage insensitive LUnAR RhoVR o, we observe no change in fluorescence (**Figure 3h**). As an additional control, perfusing FCCP, which transports protons across membranes down their concentration gradient,<sup>41</sup> rather than  $[\text{K}^+]$ , results in minimal changes in fluorescence (**Figure S12**). This supports localization of LUnAR RhoVR1 to the ER, rather than mitochondria, and corroborates colocalization data (**Figure 2**, **Figure S6-8**), since

we previously established that low doses of FCCP (500 nM) cause a change in the mitochondrial membrane potential.<sup>9</sup> It further corroborates that the fluorescence changes we observe upon switching  $[\text{K}^+]$  result from membrane potential changes in the ER, rather than off-target pH sensing, since the pH of the ER is similar to the cytosol,<sup>4</sup> while the pH gradient between the cytosol and other organelles like mitochondria and lysosome is much steeper.<sup>4, 42</sup> Taken together, these results demonstrate that LUnAR RhoVR1 is able to sense voltage transients in the ER.

We next use LUnAR RhoVR1 to examine two physiological processes in which ER membrane potential changes may play a role:  $\text{Ca}^{2+}$  release from ER stores and electrical coupling between the ER and plasma membranes. We first examine ER voltage changes during  $\text{Ca}^{2+}$  release. The ER and sarcoplasmic reticulum (SR) are major cellular stores of calcium ions.<sup>43</sup> During cellular signaling processes,  $\text{Ca}^{2+}$  channels in the ER/SR open and  $\text{Ca}^{2+}$  is released from these internal stores,<sup>43</sup> moving down its electrochemical gradient and into the cytosol.<sup>44</sup>

The movement of  $\text{Ca}^{2+}$  out of the ER down its electrochemical gradient results in negative potentials in the ER lumen relative to the cytosol, unless cations enter the ER lumen to balance the charge. Potassium may flow into the ER lumen from the cytosol to compensate for the outward flow of  $\text{Ca}^{2+}$ . Previous reports find that SR membrane potential does not change during  $\text{Ca}^{2+}$  release.<sup>45-46</sup> However, the fluorescent reporters used in these experiments have limited time resolution due to their slower kinetics.<sup>47-49</sup> VoltageFluors, because of their PeT mechanism, sense rapid changes in membrane potential,<sup>28, 50</sup> and thus we saw an opportunity to extend the conclusions of prior work by looking for evidence of rapid changes in ER membrane potential in a non-excitable cell line.

Histamine treatment induces  $\text{Ca}^{2+}$  oscillations in HeLa cells which necessitates release of  $\text{Ca}^{2+}$  from internal stores.<sup>51</sup> By simultaneously measuring ER membrane potential in HeLa cells with LUnAR RhoVR1/Cer-TCO at 200 Hz (**Figure 4a**) and  $\text{Ca}^{2+}$  oscillations via Oregon Green BAPTA (OGB, **Figure 4b**), we were able to look for rapid changes in ER voltage that could be linked to  $\text{Ca}^{2+}$  release. Intact cells were treated with Cer-TCO and LUnAR RhoVR1 to label ER and OGB (**Figure 4ab**) and stimulated with histamine to evoke  $\text{Ca}^{2+}$  release. Fluorescence traces were then aligned so that the steepest increase in OGB fluorescence is synced to  $t = 0$  in all traces (**Figure S13**). We observe no change from the baseline fluorescence of LUnAR RhoVR1 during histamine-evoked  $\text{Ca}^{2+}$  release when examining either individual cells (**Figure 4c**) or average responses across multiple trials (**Figure 4d**).

To establish a limit of detection, we developed an automated analysis routine (**Figure S13**). We examined each cell region of interest (ROI) to search for any cell on a coverslip that has a fluorescence change 10 standard deviations above the noise during the RhoVR recording. We then

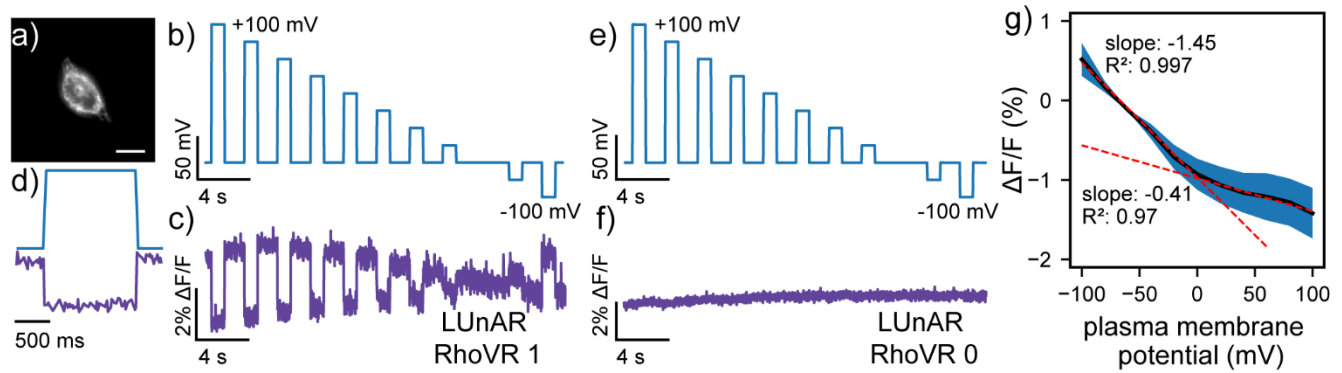


**Figure 5.** Voltage imaging with LUnAR RhoVRs in the ER under whole-cell patch-clamp conditions. **a)** Widefield fluorescence image of HeLa cell treated with Cer-TCO, followed by LUnAR RhoVR 1. **b)** Plot of command voltage vs. time for patch-clamped HeLa cells with LUnAR RhoVR 1 labeling. **c)** Plot of LUnAR RhoVR 1 fluorescence vs. time for patch-clamped HeLa cells. **d)** Zoomed-in overlay of voltage command (blue) and LUnAR RhoVR 1 response (magenta) from panels b/c. **e)** Plot of command voltage vs. time for patch-clamped HeLa cells with LUnAR RhoVR 0 labeling. **f)** Plot of LUnAR RhoVR 0 fluorescence vs. time for patch-clamped HeLa cells. **g)** Plot of percent change in fluorescence from fluorescence at -60 mV as a function of plasma membrane potential from  $n=5$  cells voltage clamped as in **a**. Error bars represent  $\pm$  S.E.M. Dashed red lines are the line of best fit for values from -100 mV to 0 mV and from +20 mV to +100 mV.

created artificial positives to test the limit of detection, increasing the fluorescence of an ROI at a single timepoint by 1 to 5% (**Figure 4e**). Then we asked what fraction of cells had detectable single-frame fluorescence changes. The unmodified data had no cells with a detectable fluorescence change, but the automated analysis could readily detect changes of 2.5% or greater ( $p < 0.001$ , Student's  $t$ -test, 2-tailed unequal variance, **Figure 4f**). Taken together, these results extend the current literature hypothesis that voltage changes during  $\text{Ca}^{2+}$  release from the ER are not electrogenic and are likely compensated for by the movement of other ions into the ER. The more rapid time sensitivity of LUnAR RhoVR<sub>1</sub> compared to existing probes rules out rapid voltage transients down to 5 ms in duration and  $<2.5\%$   $\Delta F/F$ . The lower time bound is due to the limits of the image collection rate rather than the limits of probe response kinetics.

To further explore the ability of LUnAR RhoVR<sub>1</sub> to measure biologically relevant voltage changes, we turned to patch-clamp electrophysiology to examine the electrical relationship between plasma membrane potential and ER membrane potential. A previous report using an internally targeted genetically-encoded voltage indicator (GEVI) gave evidence for electrical coupling between the plasma membrane and the ER in HEK cells and hippocampal neurons.<sup>7</sup> However, these results may be confounded by non-selective localization of the GEVI. Additionally, the orientation of the GEVI in intracellular membranes is unknown; therefore, the direction of fluorescence change cannot be used to determine the direction of the voltage change. We set out to extend these results into another cell line through simultaneous electrical measurements of plasma membrane potential and optical measurements of ER membrane potential with LUnAR RhoVR 1. We induced plasma membrane depolarization (more positive inside) and hyperpolarization (more negative inside) in LUnAR RhoVR<sub>1</sub> / Cer-TCO stained cells using whole-cell voltage clamp (**Figure 5a**).

Depolarizing steps in the plasma membrane (more positive potentials, **Figure 5b**) are accompanied by decreases in LUnAR RhoVR<sub>1</sub> fluorescence (**Figure 5c**), which corresponds to a depolarization of the ER lumen (more positive on the inside). This result is consistent with  $[\text{K}^+]$  perfusion experiments (**Figure 3**) and, along with the  $[\text{K}^+]$  perfusion calibration, provides the first unambiguous confirmation of the correspondence of the sign of membrane potential change between ER and PM membrane potentials. Depolarization at the PM results in depolarization of the ER.

Notably, the fluorescence response of LUnAR RhoVR<sub>1</sub> exactly follows the time course of the plasma membrane voltage command (**Figure 5d**, zoom-in of a single voltage step), suggesting a direct, or tight coupling of ER-PM potentials. When cells are stained with voltage insensitive LUnAR RhoVR<sub>0</sub>, the fluorescence does not change with membrane potential (**Figure 5e/f**), confirming that the observed fluorescence change with LUnAR RhoVR 1 is a response to ER membrane potential.

Finally, a plot of the change in LUnAR RhoVR 1 fluorescence in the ER ( $\Delta F/F$ ) vs. the plasma membrane potential command reveals a plot with a substantial deviation from linearity. This is in contrast to the voltage sensitivity of pre-formed LUnAR RhoVR 1 on the plasma membrane of patch-clamped HEK cells, which shows a linear relationship between  $\Delta F/F$  and plasma membrane command voltage (**Figure S5e**).

The  $\Delta F/F$  response of LUnAR RhoVR 1 in the ER appears to have two linear components. At negative plasma membrane potentials ( $\leq 0$  mV), we find a linear response of -1.4% per 100 mV ( $\pm 0.39$ , S.E.M.,  $n = 5$ ,  $R^2 = 0.997$ , **Figure 5g**). However, at positive potentials ( $> 0$  mV), the  $\Delta F/F$  voltage dependence becomes shallower: -0.4% per 100 mV ( $\pm 0.12$ , S.E.M.,  $n = 5$ ,  $R^2 = 0.97$ , **Figure 5g**). This greater than 3-fold change in the response at negative vs positive potentials is statistically significant ( $p = 0.037$ , paired  $t$ -test,  $n = 5$ , **Figure S14**). Because the fluorescence response

of pre-formed LUnAR RhoVR on the plasma membrane is linear with respect to voltage (**Figure S5e**), this non-linear behavior may be due to underlying voltage changes in the ER. An intriguing possibility is that the ER rectifies, or opposes, plasma membrane potential commands at values more positive than 0 mV, and investigations are underway to explore the cellular and molecular mechanisms underlying this observation.

In this work, we report a new small-molecule sensor capable of targeting subcellular membranes. We show that LUnAR RhoVR is capable of targeting the ER of living cells and reporting on membrane potential fluctuations in this organelle. Using dual plasma membrane patch clamp and ER voltage imaging (**Figure 5**), we corroborate previous observations showing correspondence between ER and PM potentials. By combining patch clamp experiments with ionic calibration (**Figure 3**) we directly establish that the directionality of the ER membrane potential change corresponds to the voltage change in the plasma membrane. We envision that LUnAR RhoVR will be an important addition to the suite of methods available for monitoring ER physiology. Partnering LUnAR RhoVR with other lipid-based HIDE probes will allow access to the physiology of additional organelles

## ASSOCIATED CONTENT

**Supporting Information.** Experimental details, supporting figures, and spectra. This material is available free of charge via the Internet at <http://pubs.acs.org>.

## AUTHOR INFORMATION

### Corresponding Author

\* [evanwmiller@berkeley.edu](mailto:evanwmiller@berkeley.edu)

## ACKNOWLEDGMENT

E.W.M. acknowledges support from the Camille Dreyfus Teacher Scholar Awards program and the NIH (R35GM119855). P.E.Z.K., J.G.M., A.M.M.G., M.X.N., and L.L. were supported in part by a training grant from the NIH (T32GM06698). L.L., N.D., and J.T. were supported by the NIH (R01GM131372 and R35GM134963 to A.S.) Confocal imaging experiments were conducted at the CRL Molecular Imaging Center, supported by the Gordon and Betty Moore Foundation. We thank Holly Aaron and Feather Ives for expert technical assistance. We thank Hasan Celik and the staff of the College of Chemistry NMR facility for expert technical assistance. Instruments in the CoC NMR Facility are supported in part by the NIH (S10OD024998).

## REFERENCES

- Grabe, M.; Oster, G., Regulation of organelle acidity. *The Journal of general physiology* **2001**, *117* (4), 329-44.
- Kirichok, Y.; Krapivinsky, G.; Clapham, D. E., The mitochondrial calcium uniporter is a highly selective ion channel. *Nature* **2004**, *427* (6972), 360-4.
- Mak, D. O.; Vais, H.; Cheung, K. H.; Foskett, J. K., Isolating nuclei from cultured cells for patch-clamp electrophysiology of intracellular Ca(2+) channels. *Cold Spring Harbor protocols* **2013**, *2013* (9), 880-4.
- Zhong, X. Z.; Dong, X. P., Lysosome electrophysiology. *Methods in cell biology* **2015**, *126*, 197-215.
- Saminathan, A.; Devany, J.; Veetil, A. T.; Suresh, B.; Pillai, K. S.; Schwake, M.; Krishnan, Y., A DNA-based voltmeter for organelles. *Nature nanotechnology* **2021**, *16* (1), 96-103.
- Matamala, E.; Castillo, C.; Vivar, J. P.; Rojas, P. A.; Brauchi, S. E., Imaging the electrical activity of organelles in living cells. *Communications biology* **2021**, *4* (1), 389.
- Sepehri Rad, M.; Cohen, L. B.; Braubach, O.; Baker, B. J., Monitoring voltage fluctuations of intracellular membranes. *Scientific reports* **2018**, *8* (1), 6911.
- Deal, P. E.; Kulkarni, R. U.; Al-Abdullatif, S. H.; Miller, E. W., Isomerically Pure Tetramethylrhodamine Voltage Reporters. *Journal of the American Chemical Society* **2016**, *138* (29), 9085-9088.
- Klier, P. E. Z.; Martin, J. G.; Miller, E. W., Imaging Reversible Mitochondrial Membrane Potential Dynamics with a Masked Rhodamine Voltage Reporter. *Journal of the American Chemical Society* **2021**, *143* (11), 4095-4099.
- Johnson, L. V.; Walsh, M. L.; Chen, L. B., Localization of mitochondria in living cells with rhodamine 123. *Proceedings of the National Academy of Sciences* **1980**, *77* (2), 990-994.
- Zielonka, J.; Joseph, J.; Sikora, A.; Hardy, M.; Ouari, O.; Vasquez-Vivar, J.; Cheng, G.; Lopez, M.; Kalyanaram, B., Mitochondria-Targeted Triphenylphosphonium-Based Compounds: Syntheses, Mechanisms of Action, and Therapeutic and Diagnostic Applications. *Chemical reviews* **2017**, *117* (15), 10043-10120.
- Wang, H.; Fang, B.; Peng, B.; Wang, L.; Xue, Y.; Bai, H.; Lu, S.; Voelcker, N. H.; Li, L.; Fu, L.; Huang, W., Recent Advances in Chemical Biology of Mitochondria Targeting. *Frontiers in Chemistry* **2021**, *9* (321).
- Gao, P.; Pan, W.; Li, N.; Tang, B., Fluorescent probes for organelle-targeted bioactive species imaging. *Chemical science* **2019**, *10* (24), 6035-6071.
- Tour, O.; Adams, S. R.; Kerr, R. A.; Meijer, R. M.; Sejnowski, T. J.; Tsien, R. W.; Tsien, R. Y., Calcium Green FAsH as a genetically targeted small-molecule calcium indicator. *Nature chemical biology* **2007**, *3* (7), 423-31.
- Bannwarth, M.; Corrêa, I. R.; Sztretye, M.; Pouvreau, S.; Fellay, C.; Aebischer, A.; Royer, L.; Ríos, E.; Johnsson, K., Indo-1 Derivatives for Local Calcium Sensing. *ACS chemical biology* **2009**, *4* (3), 179-190.
- Kamiya, M.; Johnsson, K., Localizable and Highly Sensitive Calcium Indicator Based on a BODIPY Fluorophore. *Analytical Chemistry* **2010**, *82* (15), 6472-6479.
- Gruskos, J. J.; Zhang, G.; Buccella, D., Visualizing Compartmentalized Cellular Mg2+ on Demand with Small-Molecule Fluorescent Sensors. *Journal of the American Chemical Society* **2016**, *138* (44), 14639-14649.
- Best, M.; Porth, I.; Hauke, S.; Braun, F.; Herten, D.-P.; Wombacher, R., Protein-specific localization of a rhodamine-based calcium-sensor in living cells. *Organic & Biomolecular Chemistry* **2016**, *14* (24), 5606-5611.
- Cañeque, T.; Müller, S.; Rodriguez, R., Visualizing biologically active small molecules in cells using click chemistry. *Nature Reviews Chemistry* **2018**, *2* (9), 202-215.
- Knall, A. C.; Slugovc, C., Inverse electron demand Diels-Alder (IEDDA)-initiated conjugation: a (high) potential click chemistry scheme. *Chemical Society reviews* **2013**, *42* (12), 5131-42.
- Chen, W.; Wang, D.; Dai, C.; Hamelberg, D.; Wang, B., Clicking 1,2,4,5-tetrazine and cyclooctynes with tunable reaction rates. *Chemical communications (Cambridge, England)* **2012**, *48* (12), 1736-8.
- Oliveira, B. L.; Guo, Z.; Bernardes, G. J. L., Inverse electron demand Diels-Alder reactions in chemical biology. *Chemical Society reviews* **2017**, *46* (16), 4895-4950.

23. Oliveira, B. L.; Guo, Z.; Boutureira, O.; Guerreiro, A.; Jiménez-Osés, G.; Bernardes, G. J., A Minimal, Unstrained S-Allyl Handle for Pre-Targeting Diels-Alder Bioorthogonal Labeling in Live Cells. *Angewandte Chemie (International ed. in English)* **2016**, *55* (47), 14683-14687.
24. Wieczorek, A.; Werther, P.; Euchner, J.; Wombacher, R., Green- to far-red-emitting fluorogenic tetrazine probes - synthetic access and no-wash protein imaging inside living cells. *Chemical science* **2017**, *8* (2), 1506-1510.
25. Wu, H.; Yang, J.; Šečková, J.; Devaraj, N. K., In situ synthesis of alkenyl tetrazines for highly fluorogenic bioorthogonal live-cell imaging probes. *Angewandte Chemie (International ed. in English)* **2014**, *53* (23), 5805-9.
26. Karver, M. R.; Weissleder, R.; Hilderbrand, S. A., Synthesis and Evaluation of a Series of 1,2,4,5-Tetrazines for Bioorthogonal Conjugation. *Bioconjugate Chemistry* **2011**, *22* (11), 2263-2270.
27. Boggess, S. C.; Gandhi, S. S.; Siemons, B. A.; Huebsch, N.; Healy, K. E.; Miller, E. W., New Molecular Scaffolds for Fluorescent Voltage Indicators. *ACS chemical biology* **2019**, *14* (3), 390-396.
28. Lazzari-Dean, J. R.; Gest, A. M.; Miller, E. W., Optical estimation of absolute membrane potential using fluorescence lifetime imaging. *eLife* **2019**, *8*.
29. Deal, P. E.; Liu, P.; Al-Abdullatif, S. H.; Muller, V. R.; Shamardani, K.; Adesnik, H.; Miller, E. W., Covalently Tethered Rhodamine Voltage Reporters for High Speed Functional Imaging in Brain Tissue. *Journal of the American Chemical Society* **2020**, *142* (1), 614-622.
30. Choy, E.; Chiu, V. K.; Silletti, J.; Feoktistov, M.; Morimoto, T.; Michaelson, D.; Ivanov, I. E.; Philips, M. R., Endomembrane trafficking of ras: the CAAX motif targets proteins to the ER and Golgi. *Cell* **1999**, *98* (1), 69-80.
31. Takakura, H.; Zhang, Y.; Erdmann, R. S.; Thompson, A. D.; Lin, Y.; McNellis, B.; Rivera-Molina, F.; Uno, S. N.; Kamiya, M.; Urano, Y.; Rothman, J. E.; Bewersdorf, J.; Schepartz, A.; Toomre, D., Long time-lapse nanoscopy with spontaneously blinking membrane probes. *Nature biotechnology* **2017**, *35* (8), 773-780.
32. Huang, Y. L.; Walker, A. S.; Miller, E. W., A Photostable Silicon Rhodamine Platform for Optical Voltage Sensing. *Journal of the American Chemical Society* **2015**, *137* (33), 10767-76.
33. Scaduto, R. C., Jr.; Grotzmann, L. W., Measurement of mitochondrial membrane potential using fluorescent rhodamine derivatives. *Biophysical journal* **1999**, *76* (1 Pt 1), 469-77.
34. Casler, J. C.; Zajac, A. L.; Valbuena, F. M.; Sparvoli, D.; Jeyifous, O.; Turkewitz, A. P.; Horne-Badovinac, S.; Green, W. N.; Glick, B. S., ESCargo: a regulatable fluorescent secretory cargo for diverse model organisms. *Molecular biology of the cell* **2020**, *31* (26), 2892-2903.
35. Stewart, M. P.; Langer, R.; Jensen, K. F., Intracellular Delivery by Membrane Disruption: Mechanisms, Strategies, and Concepts. *Chemical reviews* **2018**, *118* (16), 7409-7531.
36. Das, A.; Brown, M. S.; Anderson, D. D.; Goldstein, J. L.; Radhakrishnan, A., Three pools of plasma membrane cholesterol and their relation to cholesterol homeostasis. *eLife* **2014**, *3*.
37. Casares, D.; Escribá, P. V.; Rosselló, C. A., Membrane Lipid Composition: Effect on Membrane and Organelle Structure, Function and Compartmentalization and Therapeutic Avenues. *International journal of molecular sciences* **2019**, *20* (9).
38. Ridsdale, A.; Denis, M.; Gougeon, P. Y.; Ngsee, J. K.; Presley, J. F.; Zha, X., Cholesterol is required for efficient endoplasmic reticulum-to-Golgi transport of secretory membrane proteins. *Molecular biology of the cell* **2006**, *17* (4), 1593-605.
39. Rossi, A. M.; Taylor, C. W., IP(3) receptors - lessons from analyses ex cellula. *Journal of cell science* **2018**, *132* (4).
40. Lichtenfels, R.; Biddison, W. E.; Schulz, H.; Vogt, A. B.; Martin, R., CARE-LASS (calcein-release-assay), an improved fluorescence-based test system to measure cytotoxic T lymphocyte activity. *Journal of immunological methods* **1994**, *172* (2), 227-39.
41. Kalbáčová, M.; Vrbacký, M.; Drahota, Z.; Melková, Z., Comparison of the effect of mitochondrial inhibitors on mitochondrial membrane potential in two different cell lines using flow cytometry and spectrofluorometry. *Cytometry. Part A : the journal of the International Society for Analytical Cytology* **2003**, *52* (2), 110-6.
42. Abad, M. F.; Di Benedetto, G.; Magalhães, P. J.; Filippin, L.; Pozzan, T., Mitochondrial pH monitored by a new engineered green fluorescent protein mutant. *The Journal of biological chemistry* **2004**, *279* (12), 11521-9.
43. Carreras-Sureda, A.; Pihán, P.; Hetz, C., Calcium signaling at the endoplasmic reticulum: fine-tuning stress responses. *Cell calcium* **2018**, *70*, 24-31.
44. Goldman, D. E., POTENTIAL, IMPEDANCE, AND RECTIFICATION IN MEMBRANES. *The Journal of general physiology* **1943**, *27* (1), 37-60.
45. Sanchez, C.; Berthier, C.; Allard, B.; Perrot, J.; Bouvard, C.; Tsutsui, H.; Okamura, Y.; Jacquemond, V., Tracking the sarcoplasmic reticulum membrane voltage in muscle with a FRET biosensor. *The Journal of general physiology* **2018**, *150* (8), 1163-1177.
46. Koshita, M.; Hotta, K., Relationship between membrane potential and calcium ion fluxes in the fragmented sarcoplasmic reticulum. *The Japanese journal of physiology* **1981**, *31* (1), 109-20.
47. Tsutsui, H.; Karasawa, S.; Okamura, Y.; Miyawaki, A., Improving membrane voltage measurements using FRET with new fluorescent proteins. *Nature methods* **2008**, *5* (8), 683-5.
48. Beeler, T. J.; Farnen, R. H.; Martonosi, A. N., The mechanism of voltage-sensitive dye responses on sarcoplasmic reticulum. *The Journal of membrane biology* **1981**, *62* (1-2), 113-37.
49. Cabrini, G.; Verkman, A. S., Potential-sensitive response mechanism of diS-C<sub>3</sub>-(5) in biological membranes. *The Journal of membrane biology* **1986**, *92* (2), 171-82.
50. Beier, H. T.; Roth, C. C.; Bixler, J. N.; Sedelnikova, A. V.; Ibey, B. L., Visualization of Dynamic Sub-microsecond Changes in Membrane Potential. *Biophysical journal* **2019**, *116* (1), 120-126.
51. Vay, L.; Hernández-Sanmiguel, E.; Santo-Domingo, J.; Lobatón, C. D.; Moreno, A.; Montero, M.; Alvarez, J., Modulation of Ca(2+) release and Ca(2+) oscillations in HeLa cells and fibroblasts by mitochondrial Ca(2+) uniporter stimulation. *The Journal of physiology* **2007**, *580* (Pt 1), 39-49.